Evidence for continuum $E0$ transitions following the decay of high spin states in ^{130}Ce

J. X. Saladin, M. P. Metlay,* D. F. Winchell, and M. S. Kaplan†
Department of Physics and Astronomy, University of Pittsburgh, Pittsburgh, Pennsylvania 15260

I. Y. Lee,‡ C. Baktash, M. L. Halbert, and N. R. Johnson
Physics Division, Oak Ridge National Laboratory, Oak Ridge, Tennessee 37831

O. Dietzsch
Instituto de Fisica, Universidade de Sao Paulo, Caixa Postal 20516, Sao Paulo, SP o1498, Brazil

(Received 27 July 1995)

The decay of high-spin states in the continuum of ^{130}Ce is studied via γ-ray and internal conversion electron spectroscopy. An electron surplus above predicted yields based on γ data is seen in coincidence with transitions in the yrast band of ^{130}Ce. We attribute this to an admixture of electric monopole ($E0$) transitions with unstretched $E2$ and $M1$ transitions between strongly interacting bands of different deformations in the continuum. The $E0$ matrix elements needed to explain this surplus are comparable in magnitude to reported $E0$ matrix elements between discrete states in neighboring nuclei.

PACS number(s): 23.20.Js, 23.20.Nx, 25.70.Jj, 27.60.+j

I. INTRODUCTION

The decay of high-spin states from the entry state to the yrast line continues to be a topic of considerable interest. The decay paths in the continuum above the yrast line have been studied in the past using continuum-γ-ray spectroscopy [1], but there remain many open questions. Very little is known about the multipolarities of interband transitions. The strengths of the various multipole components are very sensitive to the deformations of the bands involved and to the softness of the total Routhian surfaces (TRS's) with respect to deformations. The present experiment was motivated by a study of Lee [2] on continuum γ rays associated with the decay of high-spin states in ^{130}Ce. In that experiment, Lee discovered a broad peak in the γ-ray continuum extending from about 100 keV to 600 keV. Anisotropy data indicated that this peak was consistent with a significant contribution from stretched dipole transitions. The present experiment was designed to study the multipolarities of these continuum transitions in more detail via internal conversion electron spectroscopy. The most significant result of this experiment is that the interpretation of the data requires a significant $E0$ component in the continuum part of the spectrum.

It should be noted that $E0$ transitions occur as a result of static or dynamic shape mixing and are an unambiguous experimental signature for shape mixing and shape coexistence. This has been demonstrated by recent experiments on $E0$ transitions in the $A\approx100$ region and the $A\approx190$ region, which have been interpreted in terms of shape mixing (see Refs. [3–8]). The importance of and ubiquitous occurrence of shape coexistence has recently been summarized by Wood *et al.* [9].

II. EXPERIMENTAL PROCEDURES AND DATA ANALYSIS

The experiment utilized the Oak Ridge Spin Spectrometer [10] with 52 NaI elements for fold selection, 18 Compton-suppressed high purity Ge detectors for γ spectroscopy, and the Pitt ICEBall, an array of five mini-orange spectrometers for electron spectroscopy [11]. High-spin states in ^{130}Ce were populated via the reaction ^{100}Mo(^{34}S,4n)^{130}Ce at a beam energy of 140 MeV using a 1.2 mg cm^{-2} self-supporting ^{100}Mo target. Energy and timing data were recorded for all detector types. For an event to be recorded it was required that more than five NaI detectors fire (fold $k>5$) and at least two Ge detectors or at least one Ge detector and one mini-orange spectrometer register a signal. About 58 x 10^6 Ge-Ge coincidence events and 30 x 10^6 Ge mini-orange events were written to tape.

To evaluate the electron spectra, it was important to carefully characterize the performance of the ICEBall, including contributions to the background. A detailed study of these properties is given in Ref. [11]. That work demonstrated that the δ-ray background decreased by over three orders of magnitude for γ-fold requirements $k>3$. Since all data were analyzed with a fold requirement $k>9$, contributions from δ rays could be neglected. The background caused by γ rays was determined on line during a run in which the Si(Li) detectors were covered with 3 mm thick Teflon sheets, which stopped the electrons. Off-line studies with sources established that this is a valid method for the determination of the γ-ray background [11]. This background accounted for about 20% of the total number of counts in the energy range between 200 and 400 keV.

γ-γ and γ-electron coincidence matrices were formed from the raw data. Figure 1(a) shows the total projection of the raw γ-γ matrix. The top curve in Fig. 1(b) is the total projection of the γ-electron matrix onto the electron energy

*Present address: Physics Department, Florida State University, Tallahassee, FL 32306.

†Present address: Department of Radiology, University of Washington Medical Center, Seattle, WA 98195.

‡Present address: Nuclear Science Division, Lawrence Berkeley Laboratory, Berkeley, CA 94720.

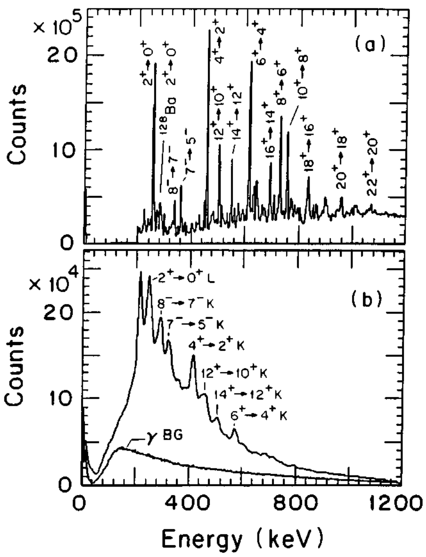

FIG. 1. (a) Total projection of the the γ-γ correlation matrix from the present work. (b) Upper curve: total projection of the raw γ-electron correlation matrix onto the electron energy axis. Lower curve: γ-ray background in the Si(Li) detector.

axis, while the bottom curve shows the γ-ray background in the Si(Li) detector.

The response functions of the Ge detectors were obtained from coincidence measurements with sources such as ^{60}Co, in which the emission of a γ ray of energy E_1 is always followed by the emission of a γ ray of energy E_2. The sources used were ^{75}Se, ^{88}Y, ^{60}Co, ^{24}Na, and ^{207}Bi, and their coincident γ rays covered the energy range from 136 to 2754 keV. From these coincidence data one can determine the response function of the Compton-suppressed Ge detectors to monoenergetic γ rays and their absolute efficiencies as a function of γ-ray energy. At each γ-ray energy, the response function was parametrized. The parametrization is illustrated in Fig. 2, which shows the response to the 1836 keV line from ^{88}Y, obtained by gating on the 898 keV line. The Compton continuum (B) and the multiple Compton events (D) were described by an expansion of eighth-degree orthogonal polynomials. This curve is shown in the figure by a solid line. The other features of the spectrum, i.e., the photopeak (A), the Compton edge (C), the singles and double escape peaks (E) and (F), the 511 keV annihilation peak (G), and the backscatter peak (H) were fitted by Gaussians. The shape of the Compton spectrum for γ rays of any energy was generated by using coefficients of expansion, which were obtained by interpolating between the measured coefficients of expansion. The peaks C to H were generated by interpolating their Gaussian parameters. The raw γ-γ matrix is then unfolded using the generated response function. The energy and efficiency calibrations were complemented by singles measurements with ^{152}Eu and ^{182}Ta sources. The unfolding procedure is illustrated in Fig. 3, which shows as an example a ^{152}Eu singles spectrum before and after unfolding. The response functions of the mini-orange spectrometers were obtained from γ-electron coincidence measurements with ^{133}Ba and ^{207}Bi sources, and singles measurements with ^{113}Sn, which has only one transition. The response function for the electron detectors is simpler than that for γ-ray detectors and consists, after the subtraction of the γ-ray background, of a flat continuum resulting from electrons that backscatter out of the detector and electrons that are scattered from various components into the detector. This continuum is again parametrized at each energy by a set of eighth order orthogonal polynomials, and the γ-electron matrix is unfolded in a way similar to that of the γ-γ matrix. Figure 4 shows ^{207}Bi spectra before and after the unfolding. The overall peak efficiency of the ICEBall is shown in Fig. 5, which is taken from [11]. It reaches a maximum of 15% of 4π at an electron energy of 360 keV and drops to about 10% at an electron energy of 240 keV. There were no calibration sources available for electron energies below 240 keV; hence only data above 240 keV were unfolded and analyzed. The projected electron spectrum of Fig. 1 shows, however, that the efficiency of ICEBall drops off very rapidly below 240

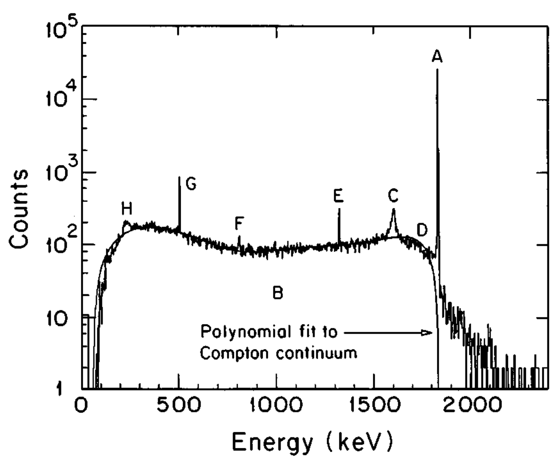

FIG. 2. Response function of a Ge detector to the 1836 keV line of ^{88}Y. Note the photo peak (A), the Compton continuum (B), the Compton edge (C), the multiple Compton events (D), the single and double escape peaks (E,F), the 511 keV annihilation peak (G), and the backscatter peak (H). The solid line represents a polynomial fit to the Compton continuum and the multiple Compton events.

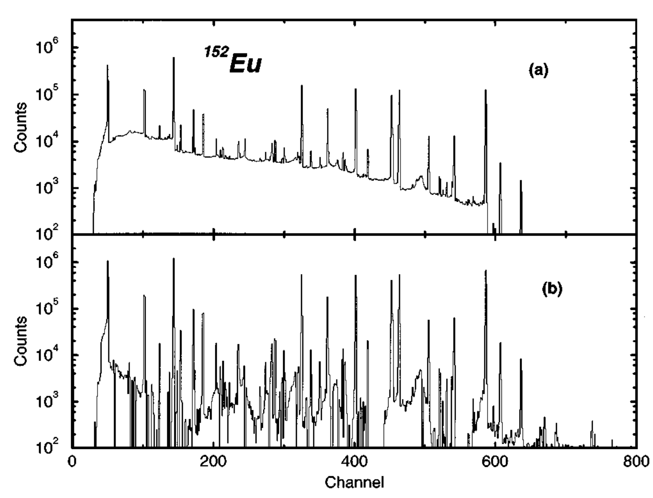

FIG. 3. The top and bottom panels show a ^{152}Eu singles spectrum before and after unfolding and peak efficiency correction.

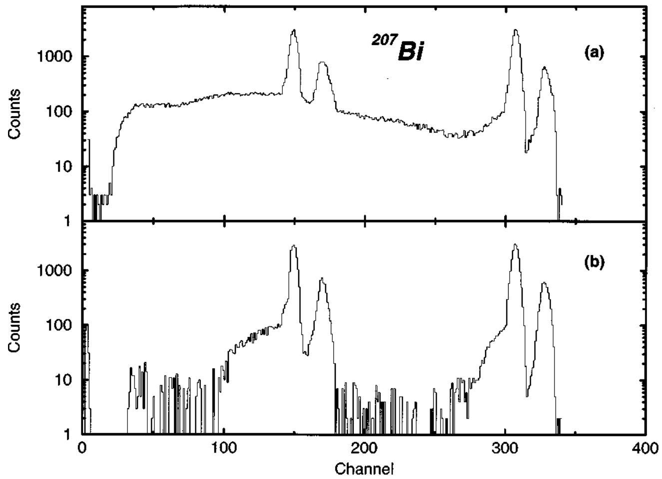

FIG. 4. The top and bottom panels show a ^{207}Bi conversion electron singles spectrum before and after unfolding.

kev. The K-conversion peak of the 2^+ to 0^+ transition corresponding to an electron energy of 214 keV is truncated on the low-energy side. This sharp cutoff is intentional in order to limit the singles rate in the Si(Li) detectors from low-energy δ rays.

To compare γ and electron spectra gated on particular γ lines, it was necessary to generate hypothetical electron spectra from the γ-ray spectra. For each γ spectrum, electron spectra were calculated assuming that the multipolarity of all transitions is either pure $M1$ or pure $E2$. For conversion from each electron shell (i.e., K, L_{I}, L_{II}, etc.) an electron spectrum was generated from the unfolded γ-ray spectrum by shifting the spectrum down by the electron binding energy and multiplying the intensity by the conversion coefficient. The total conversion electron spectrum was obtained by summing the individual spectra. This spectrum was then convolved with the measured resolution function of the experimental electron spectra. The electron spectra were normalized such that the peak areas corresponding to known $E2$ transitions agreed with the corresponding areas derived from the γ-γ matrices. The normalization factors for spectra resulting from different gates varied by up to 15%. However, the analysis was carried out using a single average normalization in order to avoid biasing the results.

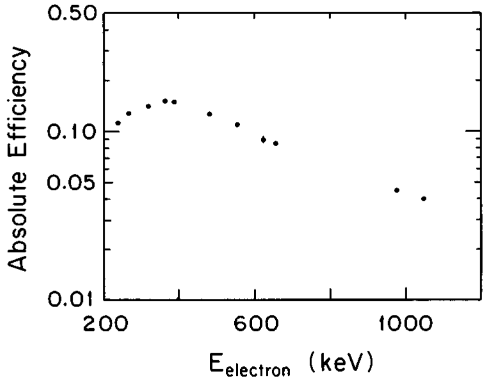

FIG. 5. Peak efficiency of the ICEBall as determined from radioactive sources (see text).

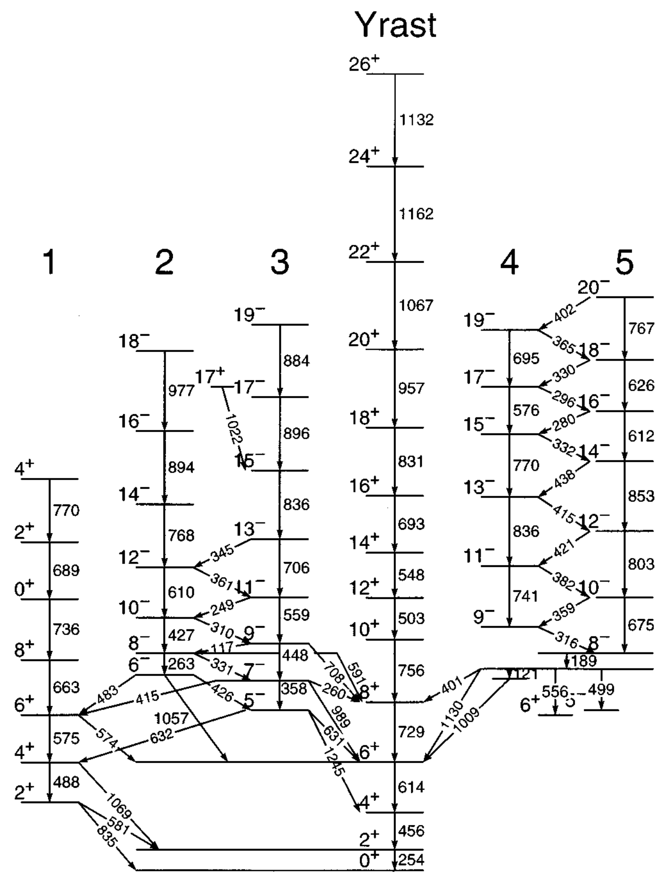

FIG. 6. Level scheme of ^{130}Ce, per Ref. [12].

III. RESULTS

Figure 6 shows, for later reference, the level scheme of ^{130}Ce as established in Ref. [12]. Figure 7 shows a comparison between the measured electron yield and calculations assuming either pure $M1$ or pure $E2$ multipolarities for γ gates on the $4^+ \rightarrow 2^+$, $8^+ \rightarrow 6^+$, $12^+ \rightarrow 10^+$, and $16^+ \rightarrow 14^+$ transitions in the yrast band. Figure 8 displays the same information for gates on the $7^- \rightarrow 5^-$, $9^- \rightarrow 7^-$, and the $11^- \rightarrow 9^-$ transitions in the most intense negative parity band, and the $2^+ \rightarrow 0^+$ transition in ^{128}Ba. The top panels in both figures show the comparison between the gated electron spectra and the electron spectra derived from the γ data. The middle and bottom panels show the difference between the measured intensities and the calculated intensities, for pure $E2$ (middle panel) or pure $M1$ (bottom panel) transitions, respectively.

To help interpret these figures it is instructive to examine the energy dependence of the K and L conversion coefficients shown in Fig. 9. For the energy range of interest, the $M1$ K-conversion coefficient is larger than the $E2$ K-conversion coefficient, and the difference between the two increases with energy. However, the total $M1$ L-conversion coefficient is considerably smaller than the total $E2$ L-conversion coefficient at low energies, but this difference decreases with increasing energy and the two coefficients cross at about 350 keV. Thus the calculated $E2$ intensity of the $2^+ \rightarrow 0^+$ L-conversion peak at 248 keV exceeds the calculated $M1$ intensity, whereas at higher energies, where the

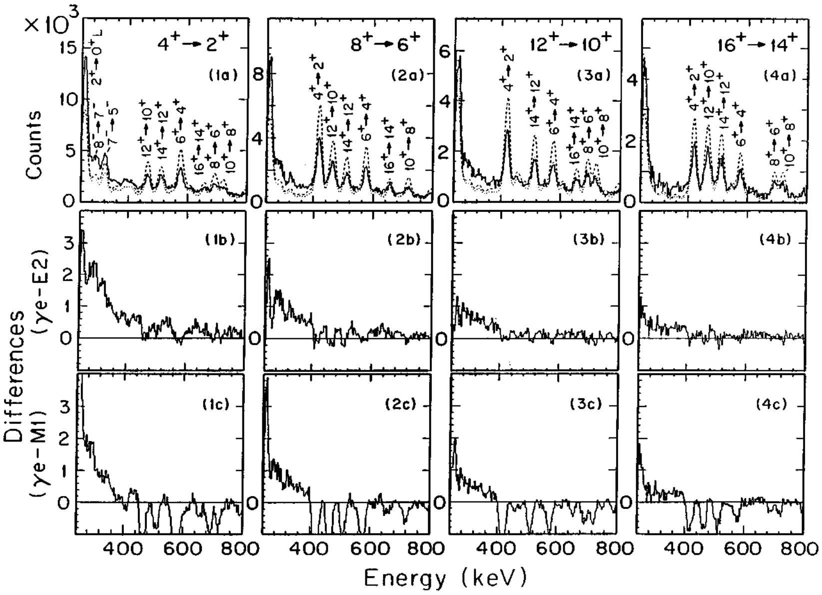

FIG. 7. The top panels show gated electron spectra (histograms) in the energy range from 240 to 800 keV. The gates are indicated at the top of each panel. The dashed and dotted lines represent the electron spectra derived from the γ-γ matrix under the assumptions of pure $M1$ and pure $E2$ transitions, respectively. The middle panels show the difference spectra obtained by subtracting the calculations based upon the assumption of pure $E2$ transitions from the measured electron spectra. The bottom panels show the analogous difference for calculations based on the assumption of pure $M1$ transitions. The scaling factor 10^3 indicated in the top left corner applies to all panels.

dominant contributions come from K conversion, the calculated $M1$ intensities exceed the calculated $E2$ intensities.

Figure 7 shows that the electron spectra gated on yrast transitions exhibit a large electron surplus above the predicted amount for pure $E2$ transitions or pure $M1$ transitions. For γ gates on the lowest four yrast transitions and electron energies below 300 keV the experimental electron intensities exceed the calculate $M1(E2)$ intensities by factors ≈ 2 (≈ 3). These surplus intensities can therefore not be explained in terms of pure or mixed $E2$ and $M1$ transitions. The surplus spectra form continua in the energy range between 240 and 400 keV. A few of the panels show, superimposed on the continuum, small peaks which are correlated with discrete peaks in the electron spectra. These peaks are caused by the slight gate dependence of the normalization, which was not taken into account in the analysis (see above). It is important to note that the continuum surplus is present in all gates on the yrast transitions in ^{130}Ce. Concentrating on $M1$ expectations, one sees in Fig. 8 a small surplus for gates on the $7^- \rightarrow 5^-$ transition in ^{130}Ce but no statistically significant surplus for gates on the $9^- \rightarrow 7^-$ and $11^- \rightarrow 9^-$ transitions and no surplus for a gate on the $2^+ \rightarrow 0^+$ transition in ^{128}Ba, which was also populated in this experiment. The negative excursions in the bottom panels of Figs. 7 and 8 at energies above 400 keV correlate, as expected, with known $E2$ transitions (see top panel), while the middle panels show vanishing intensity at the corresponding positions. Examination of the middle and bottom panels indicates that all transitions above 400 keV can be explained in terms of pure $E2$ or mixed $E2+M1$ transitions.

The results from all gated spectra (including spectra not shown) are summarized in Table I. Column 5 lists the difference $(I_{\mathrm{expt}} - I_{M1})$ between the experimental number of counts I_{expt} and the number of counts predicted for pure $M1$ transitions, I_{M1}, in the electron energy range from 265 to 395 keV; column 6 gives the analogous quantity for $E2$ predictions. The quoted uncertainties contain contributions from statistics, the normalization between the electron and γ spec-

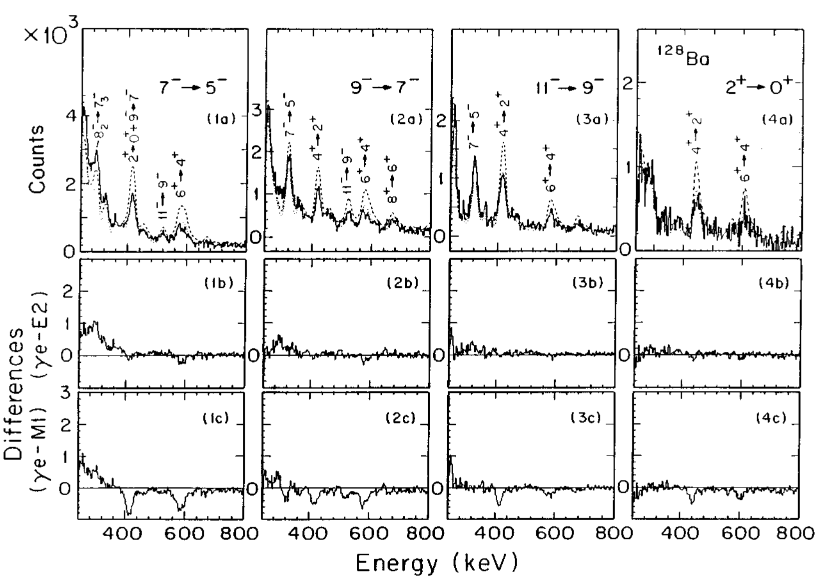

FIG. 8. Same as Fig.7 for different transitions, as indicated in the panels.

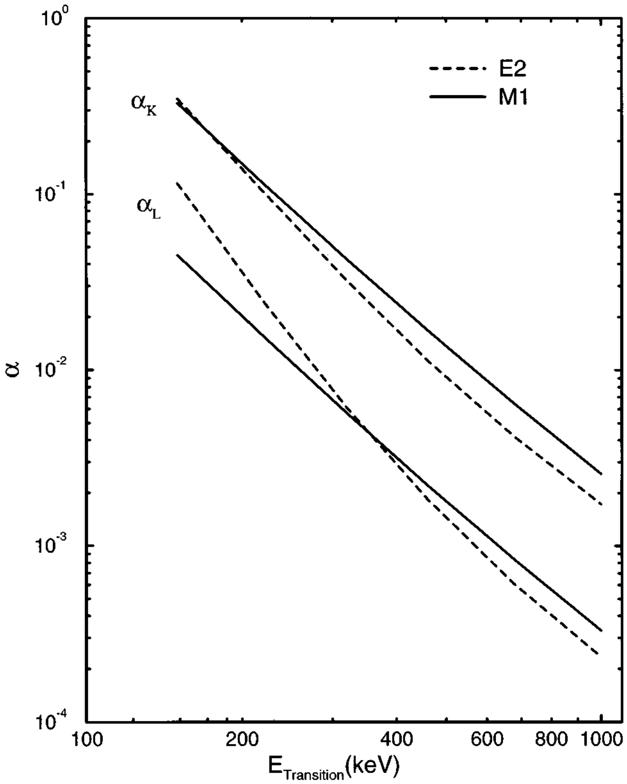

FIG. 9. K- and L- conversion coefficients for $M1$ and $E2$ transitions in Ce.

tra, and uncertainties associated with the unfolding process. These contributions were added in quadrature. In addition to the large surpluses in the yrast-gated spectra, there are indications of small surpluses in coincidence with two transitions in the negative parity band and in the $19/2^- \rightarrow 15/2^-$ transition in ^{127}Ba. However, no statistically significant surplus is observed in coincidence with any other gamma transition in ^{130}Ce or in gates on ^{128}Ba, ^{130}La, or ^{131}Ce. These findings provide convincing evidence that the surplus electrons result from physical processes in the decay of high-spin states in ^{130}Ce rather than from instrumental effects or extranuclear effects such as the δ-ray background. Figure 10 shows the surplus intensity for the spectra gated on yrast transitions in ^{130}Ce as a function of the gating transition. The abscissa represents the initial spin of the gating transition. Starting with spin 8 there is a drop in intensity with increasing spin. This suggests that the states from which the surplus electrons originate feed into the yrast band above spin 8. We propose that these surplus electrons result from $E0$ transitions in ^{130}Ce.

IV. DISCUSSION

There is strong experimental and theoretical evidence that nuclei in the $A \approx 130$ mass region are soft with respect to both β and γ deformations and develop, with increasing an-

TABLE I. Column 2 gives initial and final spins and parities of gating transition. The subscripts refer to band numbers as defined in Fig. 6. Column 3 gives the transition energy and column 4 the excitation energy of the initial state. Columns 5 and 6 are defined in the text.

	$I_i^\pi \rightarrow I_f^\pi$	$E_i - E_f$ (keV)	$E(I_i)$ (keV)	$M1$ surplus (counts/10^3)	$E2$ surplus (counts/10^3)
^{130}Ce	$2^+ \rightarrow 0^+$	254	254	41.8 (58)	84.6 (13)
yrast	$4^+ \rightarrow 2^+$	457	711	49.5 (79)	75.6 (91)
band	$6^+ \rightarrow 4^+$	614	1325	58.2 (99)	82.2 (86)
	$8^+ \rightarrow 6^+$	729	2054	33.1 (56)	42.5 (77)
	$10^+ \rightarrow 8^+$	757	2811	28.8 (40)	32.2 (52)
	$12^+ \rightarrow 10^+$	503	3314	24.1(43)	30.8 (49)
	$14^+ \rightarrow 12^+$	549	3863	13.9(21)	17.6 (30)
	$16^+ \rightarrow 14^+$	693	4556	14.3 (30)	17.0 (34)
^{130}Ce	$7^- \rightarrow 5^-$	359	2315	11.9 (13)	27.7 (42)
negative parity	$9^- \rightarrow 7^-$	448	2763	−2.2 (7)	11.2 (23)
band 3	$11^- \rightarrow 9^-$	559	3322	2.10 (84)	7.8 (14)
^{130}Ce	$8_1^+ \rightarrow 6_1^+$	664	2563	0.61 (91)	6.4 (22)
other	$10_2^- \rightarrow 8_2^-$	428	3074	−3.7 (52)	0.24 (7)
transitions	$5_3^- \rightarrow 6_y^+$	631	1956	−0.7 (22)	12.1 (30)
	$8_2^- \rightarrow 7_3^-$	331	2646	−1.90 (59)	−7.7 (71)
^{130}La	$12^+ \rightarrow 11^+$	314	688+x	−4.8 (14)	−3.0 (20)
^{128}Ba	$2^+ \rightarrow 0^+$	284	284	−0.02 (1)	6.2 (22)
^{131}Ce	$15/2^- \rightarrow 11/2^-$	510	810	−3.0 (13)	3.2 (18)
^{127}Ba	$19/2^- \rightarrow 15/2^-$	645	1422	5.21 (89)	11.0 (28)

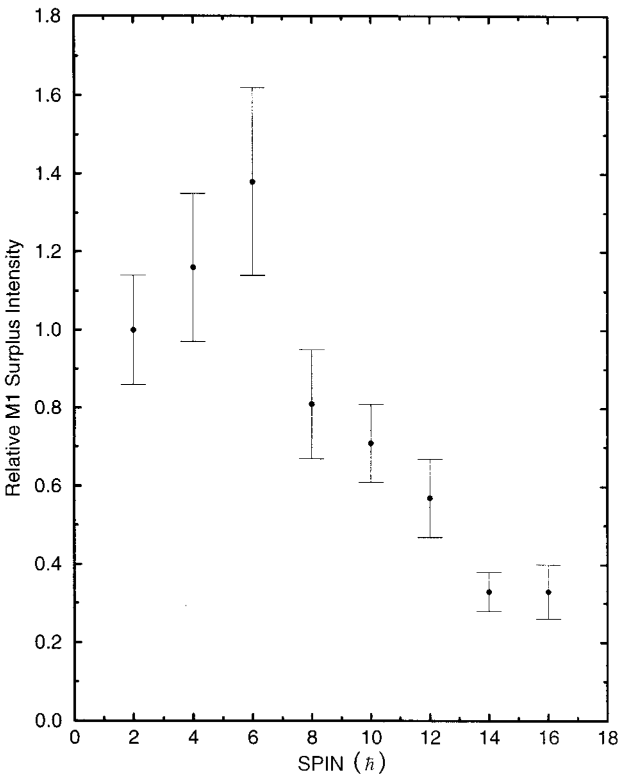

FIG. 10. Surplus intensity for gates on yrast transitions. The abscissa labels the initial spin of the gating transition.

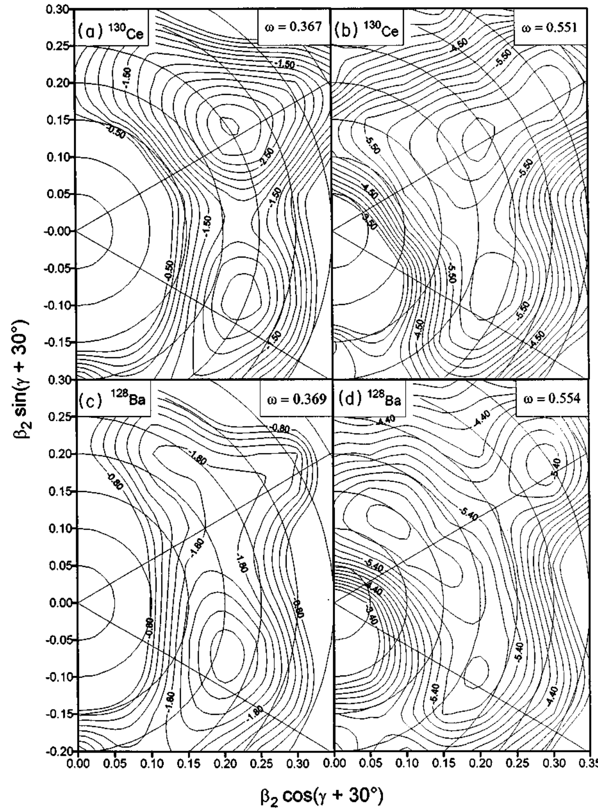

FIG. 11. Total Routhian surfaces for ^{130}Ce and ^{128}Ba. The distance between equipotential lines is 0.2 MeV.

gular velocity, coexisting states with different shapes [12–14]. The theoretical evidence is based on cranked Woods-Saxon-Bogoliubov calculations and is illustrated in panels (a) and (b) of Fig. 11, which shows total Routhian surfaces for ^{130}Ce at angular frequencies $\hbar\omega$ of 0.37 and 0.55 MeV. At $\hbar\omega$=0.37 MeV the lowest minimum is prolate collective and corresponds to a nearly axially symmetric deformation with β=0.25 and $\gamma=+3°$. This minimum is soft in the direction of increasing β. An additional collective oblate minimum is at β=0.24 and $\gamma=-52°$. At $\hbar\omega$=0.55 MeV a new prolate collective minimum develops with β=0.33 with $\gamma\approx 0$. At $\hbar\omega$=0.6 MeV this minimum becomes yrast. This shape transition can be traced to the change in configuration whereby the deformation-driving highly aligned $i_{13/2}$ neutron orbitals become occupied. The two prolate coexisting minima can lead to the formation of strongly interacting bands, as indicated schematically in Fig. 12, which are built on orthogonal combinations of wave functions

$$\Psi_1 = a|\beta_1\rangle + b|\beta_2\rangle, \tag{1}$$

$$\Psi_2 = -b|\beta_1\rangle + a|\beta_2\rangle, \tag{2}$$

with different deformations β_1 and β_2. In the following we assume that the mixing amplitudes a and b are normalized, i.e., $a^2+b^2=1$. It is customary to express theoretical predictions for $E0$ transitions between two states in terms of the dimensionless matrix element

$$\rho(E0) = \frac{1}{eR^2}\langle I,i|E0|I,f\rangle, \tag{3}$$

where R is the nuclear radius. The monopole operator $E0$ acts on protons only and is given by $E0 = e\Sigma_{p=1}^{Z} r_p^2$. For the band mixing model the matrix element $\rho(E0)$ is given by [3,4]

$$\rho(E0) = \frac{3Z}{4\pi}ab(\beta_1^2 - \beta_2^2). \tag{4}$$

An alternative possibility is the existence of bands built on vibrational excitations (dynamic shape mixing) in the β-soft minimum which then decay into bands of stable deformation. As an estimate for the magnitude of $\rho(E0)$ one may take the expression for $E0$ transitions between the β-vibrational band and the ground band [15],

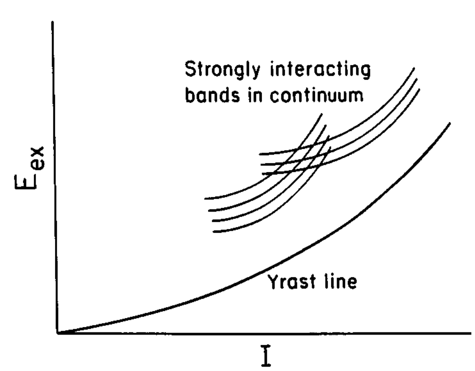

FIG. 12. Schematic illustration of interacting bands that may give rise to a significant $E0$ component in interband transitions.

$$\rho(E0;I,n_\beta=1\rightarrow I,n_\beta=0)=\frac{3Z}{2\pi}\beta_0(\beta-\beta_0), \qquad (5)$$

in which β_0 and $(\beta-\beta_0)$ are the equilibrium deformation and the amplitude of the oscillation, respectively. This expression is valid in the adiabatic approximation, where there is no coupling between the rotational and vibrational motion.

It is possible to extract estimates for the magnitude of the $E0$ matrix elements from the experiments, and to compare these estimates with measured matrix elements for discrete transitions in neighboring nuclei. If we assume that the $I\rightarrow I$ transitions responsible for the production of $E0$ transitions are of mixed $E0+M1+E2$ character, then the total probability for the emission of electrons can be expressed as [16]

$$\Gamma_e=\Gamma_{e,E0}+\Gamma_\gamma\left[\alpha(M1)\frac{1}{1+\delta^2}+\alpha(E2)\frac{\delta^2}{1+\delta^2}\right], \qquad (6)$$

where δ^2 is the $E2/M1$ mixing ratio. In the following we consider two limiting cases: admixture of $E0$ and $M1$ only ($\delta^2=0$) and admixture of $E0$ and $E2$ only ($\delta^2=\infty$). We may then extract the intensity ratios $[\Gamma_{E0}/\Gamma_{e,M1}]_{\mathrm{expt}}$ or $[\Gamma_{E0}/\Gamma_{e,E2}]_{\mathrm{expt}}$ from the experimental data. These ratios can be related to the reduced transition matrix elements for the two limiting cases, according to the equations

$$\left[\frac{\Gamma_{E0}}{\Gamma_{e,M1}}\right]_{\mathrm{expt}}=F_{M1}(K)\frac{|\langle I_f\|E0\|I_i\rangle|^2}{|\langle I_f\|M1\|I_i\rangle|^2} \qquad (7)$$

and

$$\left[\frac{\Gamma_{E0}}{\Gamma_{e,E2}}\right]_{\mathrm{expt}}=F_{E2}(K)\frac{|\langle I_f\|E0\|I_i\rangle|^2}{|\langle I_f\|E2\|I_i\rangle|^2}, \qquad (8)$$

where K is the transition energy. The functions F_{M1} and F_{E2} are given in the Appendix. They depend upon conversion coefficients and the factors $A(E0)$ which enter into the calculations of $\Gamma_{e,E0}$ [17]. Making reasonable assumptions about the magnitude of the interband $M1[E2]$ matrix elements, one can extract from Eq. (7) [8] $E0$ matrix elements. From the systematics of the region [18], we assume $\langle M1\rangle^2\approx0.02\mu_N^2$ and $\langle E2\rangle^2\approx400e^2\mathrm{fm}^4$. Estimates based on our data and experimental results from discrete transitions in this region [15,16] are compared in Table II . It should be noted that the $E0$ matrix elements required to explain our data are comparable in magnitude to those between discrete states in neighboring nuclei and do not require unreasonable assumptions about the values of β_1, β_2, and $(\beta_1-\beta_2)$ or β_0 and $(\beta-\beta_0)$. It is illustrative to estimate the mixing amplitudes a and b required for a matrix element $\rho(E0)=0.25$ which is near the upper limit required to explain the experimental data. Assuming $\beta_1=0.25$ and $\beta_2=0.35$ as suggested by the TRS plots of Fig. 11 one obtains, from Eq. (4), $a=0.95$ and $b=0.32$, which represents a rather small amount of mixing. Table II illustrates that the largest experimental estimates are close to the values observed for discrete $E(0)$ transitions between β-vibrational states and ground-band states. It is noteworthy that the TRS landscape of the ^{128}Ba nucleus (in which no surplus electrons were detected) differs drastically from that of ^{130}Ce. It is rather structureless, with no well-defined minima.

TABLE II. Results of the present ^{130}Ce experimental estimates for $\rho(E0)$, compared with experimental data on known discrete $E0$ transitions in nearby nuclei. Data on known transitions are from Refs. [9] and [12].

Nucleus	Transition	E (keV)	$\rho(E0)$
^{130}Ce	continuum	$\approx$ 275–440	$\approx$0.06–0.15
			$(E0+E2$ limit)
	(present work)		$\approx$ 0.12–0.29
			$(E0+M1$ limit)
^{114}Cd	$2_2^+\rightarrow2_g^+$	651	$\leqslant$0.09
	$4_2^+\rightarrow4_g^+$	449	0.057
	$4_4^+\rightarrow4_2^+$	633	0.12
^{116}Sn	$0_2^+\rightarrow0_1^+$	271	0.32±0.04
^{118}Sn	$0_2^+\rightarrow0_1^+$	299	0.1±0.37
^{150}Sm	$2_\beta^+\rightarrow2_g^+$	712	0.22±0.07
	$2_3^+\rightarrow2_g^+$	860	0.047
^{152}Sm	$0_2^+\rightarrow0_1^+$	398	$\leqslant$0.09
	$2_\gamma^+\rightarrow2_g^+$	964	0.029±0.04
	$4_\gamma^+\rightarrow4_g^+$	1006	0.09±0.04
	$8_\beta^+\rightarrow8_g^+$	541	0.205±0.06
	$10_\beta^+\rightarrow10_g^+$	495	0.28±0.1

It should be noted that evidence for continuum $E0$ transitions in ^{143}Eu has recently been reported in Ref. [19]. This experiment was based on measurements of the multiplicity of K x rays originating from the conversion of quasicontinuum transitions. The authors interpret the large observed multiplicity in terms of unexpectedly large $M1$ strength in the quasicontinuum or, alternatively, in terms of low-energy $E0$ transitions associated with shape changes in the quasicontinuum.

V. SUMMARY AND CONCLUSIONS

In this experiment an excess in the intensity of internal conversion electrons was established in the decay of high-spin states in ^{130}Ce. This excess forms a continuum between 240 keV and 390 keV and cannot be explained in terms of mixed or pure $M1$ and $E2$ transitions. It is strongly correlated with yrast transitions in ^{130}Ce and feeds into the yrast band at spins $I\geqslant8$. The excess is not correlated with all bands in ^{130}Ce and no excess was found in the isotopes ^{128}Ba and ^{130}La, which were also populated in this experiment. We propose that the excess is caused by $E0$ transitions in the quasicontinuum of ^{130}Ce and suggest two schematic models. Future experiments are planned to search for the origin of these conversion electrons in the (E_x,I) plane and to investigate the systematics of $E0$ transitions in the $A\approx$ 130 region. The experiment also establishes that a high-efficiency array of miniature orange spectrometers, such as ICEBall, in combination with a large array of Ge detectors permits on-line discrete and continuum γ-electron coincidence spectroscopy. Such combined arrays will be powerful tools for the determination of the multipolarity of electromagnetic transitions, and they provide the only means to detect $E0$ transitions, which are signatures of shape mixing.

ACKNOWLEDGMENTS

The authors wish to thank M. A. Riley, A. Virtanen, and the staff of the ORNL Holifield Heavy Ion Research Facility for their assistance with the Spin Spectrometer. We are very grateful to J. Walton from the Lawrence-Berkeley Laboratory, who made the Si(Li) detectors used in this experiment. Special thanks are due to Professor C. M. Vincent for many insightful comments and discussions. We thank W. Nazarewicz from ORNL and R. Wyss from the Royal Institute of Technology in Stockholm for providing us with the data base from which the TRS's were extracted. We are indebted to Dr. F. Cristancho for helpful comments. This research was funded by the National Science Foundation (Grant No. PHY-9022196) and the Department of Energy (Contract No. DE-AC05-84OR21400).

APPENDIX

The $E0$ decay rates corresponding to the emission of $K, L_{\mathrm{I}}, L_{\mathrm{II}}, \ldots$ electrons can be written as the product of a function $A(E0)$ which depends on electronic wave functions only and the square of the dimensionless matrix element $\rho(E0)$ which depends on the nuclear wave function only [17], i.e.,

$$\Gamma_{E0} = \frac{8\pi\alpha K}{2I+1} A(E0)\rho^2(E0). \tag{A1}$$

Here α and K are the fine-structure constant and the transition energy. The functions $A(E0)$ for the emission of $K, L_{\mathrm{I}}, L_{\mathrm{II}}, \ldots$ electrons have been tabulated (in natural units) by Hager and Selzer [17]. A convenient expression for Γ_{E0} is

$$\Gamma_{E0} = (2.786\times 10^{20}) A(E0) \frac{K}{2I+1} \rho^2(E0), \tag{A2}$$

where K is in MeV, $A(E0)$ is in natural units as tabulated in Ref. [17], and Γ_{E0} is in sec^{-1}. Similar equations are known for magnetic dipole and electric quadrupole decay rates [20]:

$$\Gamma_{\gamma,M1} = 1.76\times 10^{13} K^3 B(M1) \tag{A3}$$

and

$$\Gamma_{\gamma,E2} = 1.22\times 10^{9} K^5 B(E2). \tag{A4}$$

Combining Eqs. (7) [8], (A2), and (A3) [(A4)] leads to expressions for $F_{M1}(K)$ and $F_{E2}(K)$,

$$F_{M1}(K) = (1.58\times 10^{7}) K^{-2} \frac{A(E0)}{\alpha(M1)} \tag{A5}$$

and

$$F_{E2}(K) = (2.28\times 10^{11}) K^{-4} \frac{A(E0)}{\alpha(E2)}. \tag{A6}$$

[1] B. Herskind, A. Bracco, R. A. Broglia, T. Dossing, A. Ikeda, S. Leoni, J. Lisle, M. Matsuo, and E. Vigezzi, Phys. Rev. Lett. **68,** 3008 (1992), and references therein.

[2] I. Y. Lee, in *High Angular Momentum Properties of Nuclei*, edited by N. R. Johnson (Harwood, Chur, Switzerland, 1983).

[3] H. Mach, M. Moszynski, R. L. Gill, G. Molnar, F. K. Wohn, J. A. Winger, and John C. Hill, Phys. Rev. C **41**, 350 (1990).

[4] K. Heyde and R. A. Meyer, Phys. Rev. C **37**, 2170 (1988).

[5] E. F. Zganjar and J. L. Wood, Nucl. Phys. **A520**, 427c (1990), and references therein.

[6] Y. Xu, K. S. Krane, M. A. Gummin, M. Jarrio, J. L. Wood, E. F. Zganjar, and H. K. Carter, Phys. Rev. Lett. **68,** 3853 (1992).

[7] J. Schwarzenberg, J. L. Wood, and E. F. Zganjar, Phys. Rev. C **45,** R896 (1992).

[8] P. Van Duppen, M. Huyse, and J. L. Wood, J. Phys. G **16,** 441 (1990).

[9] J. L. Wood, K. Heyde, W. Nazarewicz, M. Huyse, and P. van Duppen, Phys. Rep. **215,** 102 (1992).

[10] M. Jääskeläinen, D. G. Sarantites, R. Woodward, F. A. Dilmanian, J. T. Hood, R. Jääskeläinen, D. C. Hensley, M. L. Halbert, and J. H. Barker, Nucl. Instrum. Methods **204,** 385 (1983).

[11] M. P. Metlay, J. X. Saladin, I. Y. Lee, and O. Dietzsch, Nucl. Instrum. Methods A **336,** 162 (1993).

[12] D. M. Todd, R. Aryaeinejad, D. J. G. Love, A. H. Nelson, P. J. Nolan, P. J. Smith, and P. J. Twin, J. Phys. G **10,** 1407 (1984).

[13] Y. S. Chen, S. Frauendorf, and G. A. Leander, Phys. Rev. C **28,** 2437 (1983).

[14] R. Wyss, J. Nyberg, A. Johnson, R. Bengtsson, and W. Nazarewicz, Phys. Lett. B **215,** 211 (1988).

[15] N. A. Voinova-Eliseeva and I. A. Mitropol'skii, Fiz. Elem. Chasits At. Yadra **17**, 173 (1986) [Sov. J. Part. Nucl. **17**, 521 (1986)].

[16] A. V. Aldushchenkov and N. A. Voinova, Nucl. Data Tables **11,** 299 (1972).

[17] R. S. Hager and E. C. Seltzer, Nucl. Data Tables A **6**,1 (1969).

[18] P. M. Endt, A. Data Nucl. Data Tables **26**, 47 (1981).

[19] M. Palacz *et al.*, Nucl. Phys. **A578,** 225 (1994).

[20] A. Bohr and B. R. Mottelson, *Nuclear Structure* (Benjamin, New York, 1969), Vol. 1, p. 382.